Hindawi
Shock and Vibration
Volume 2020, Article ID 5416267, 11 pages
https://doi.org/10.1155/2020/5416267

Research Article

Analysis on the Effects of Material Parameters on the Fatigue Performance of Novel Anticorrugation Elastic Rail Clips

Ping Wang[1,2] **Jun Lu**[1,2] **Caiyou Zhao**[1,2] **Li Yao**[1,2] **and Xuanhui Ming**[1,2]

[1]*School of Civil Engineering, Southwest Jiaotong University, Chengdu, China*
[2]*Key Laboratory of High-speed Railway Engineering, Ministry of Education, Chengdu, China*

Correspondence should be addressed to Caiyou Zhao; zcy_swjtu@yeah.net

Received 29 November 2019; Accepted 9 January 2020; Published 10 February 2020

Academic Editor: Alvaro Cunha

A novel elastic rail clip was obtained through size improvement based on the II-type elastic rail clips to solve the fatigue failure of elastic rail clips. The metro vehicle-track coupling model and the fastener system refinement model were developed to analyze the effects of the material (38Si7 and 60Si2Mn) on the static and dynamic responses of the elastic rail clips and their fatigue performances under rail corrugation. According to the results, the elastic rail clip made of 60Si2Mn did not undergo any plastic deformation and exhibited higher strength than that made of 38Si7. Elastic rail clips made of 38Si7 and 60Si2Mn presented a consistent clamping force, natural frequency, and vibration acceleration. However, they were most sensitive to the wavelength of 50 mm. Both materials influenced the small back bending area of the elastic rail clip only. The elastic rail clip made of 60Si2Mn could meet the fatigue life requirements of 5 million times. As for the elastic rail clip made of 38Si7, the corresponding values of corrugation with the wavelength of 50 mm and 40 mm are to be controlled below 0.09 mm and 0.41 mm, respectively. The performance of the elastic rail clips to resist rail corrugation can be improved significantly through the increase in the geometric dimensions and selection of materials with higher strength.

1. Introduction

As the most important part of the track structure, the fastener system is a key unit that connects the rail and the subrail foundation. As a component of clamping rail, the elastic clip is one of the most important parts of the fastener system. Due to the rapid increase in the quantity of rail traffic systems constructed in China, the problems of vibration and noise caused by trains are of great concern. Recently, many broken elastic rail clips have been found in subway lines, and the fatigue failure of elastic rail clips is often accompanied by short-pitch rail corrugation [1], which is a severe threat to the traffic safety. Therefore, there is an urgent need to optimize the size of the existing elastic rail clips and also for better materials selection for the elastic rail clips. Future studies on the fatigue life of novel elastic rail clips under short-pitch rail corrugation are recommended; as well, the fatigue performance could be evaluated.

Several studies on the optimal design and fatigue performance of elastic rail clips have been reported. In respect to the optimal design of elastic rail clips, Xiao and Zhao [2] proposed the measurement indices for the optimal design of elastic rail clips and the optimal design methods, in terms of energy. Yang and Pan [3] compared and analyzed the influence of different materials on the static properties of elastic rail clips. Li et al. [4] studied the design parameter sensitivity of ω-type elastic rail clips and the optimal design methods of elastic rail clip parameters. Hu et al. [5] set a W1-type elastic rail clip for high-speed railways as a tool to study the influence of its geometric parameters on the clamping force and maximum stress. The results demonstrate that the performance of elastic rail clips can be greatly improved by increasing the projectile path T, diameter d, arch span L0, and the back bending area $R2$, or by reducing the clamping area b2.

In the aspect of studies on the fatigue failure of elastic rail clips, Mohammadzadeh et al. [6, 7] built a vehicle-track

coupling model and a finite element model of SKL14 elastic rail clips. The crack initiation life of the elastic rail clips was also analyzed using the rain flow counting method and the Palmgren–Miner linear damage rule. Also, Hasap et al. [8, 9] analyzed the effects of clamping force and deformation on the fatigue life of the elastic rail clip through fatigue tests and applied the Goodman diagram in evaluating the fatigue performance of elastic rail clips. Xiao et al. [10] also established a refined fastener system model and conducted a modal and harmonic response analysis of the fastener system under operation. By combining the vibration acceleration of the elastic rail clip measured in situ, they presumed that the resonance of elastic rail clips triggered by rail corrugation is the primary cause of failure of elastic rail clips. Ferreño et al. [11] proposed fatigue prediction for the SKL-1 elastic rail clip via the fatigue test and finite element method and analyzed the rationality of the heating processing technology and field installation accuracy for elastic rail clip materials.

In previous studies, the static performance of elastic rail clips was mainly considered as the optimal design objective, whereas the fatigue performance was often ignored. On the other hand, studies on the fatigue performance of elastic rail clips mainly focused on the effects of simulation calculations and external incentives on the fatigue performance of elastic rail clips, the influence of the parameters of elastic rail clips seldom considered. Therefore, a novel fastener system whose elastic rail clip is improved based on the II-type elastic rail clip is proposed in this paper. The two-dimensional structure of this elastic rail clip is shown in Figure 1. Compared with the dimensional parameters of the II-type elastic rail clip, its arch span, L, arch rise, H, arc bending radius, $R2$, and diameter, d of the proposed system increased by 10 mm, 5 mm, 2.5 mm, and 1 mm, respectively. In this study, the subway vehicle-track coupling model and the fastener system refinement model were developed. The bilinear kinematic hardening model was employed to describe the stress-strain relation of the elastic rail clip material in stages. The vibration acceleration and the stress-time history curves of the elastic rail clip were obtained by cosimulation calculations. By combining fatigue analysis and cumulative damage theory, we studied the effects of clip material on the fatigue life of the elastic rail clip under rail corrugation. This study provides references for the optimal design and anti-corrugation design of elastic rail clips.

2. Calculation Model and Method of the Fatigue Life of Elastic Rail Clips in the Fastener System

To calculate the fatigue life of fastener elastic rail clips, the numerical model and the analytical method for the fatigue life of elastic rail clips in the fastener system are established. The elastic rail clip is a part of the fastener system, which provides flexibility to the wheel-rail system. Taking into account the excessive complexity of characterization and prediction of elastic rail clips in the wheel-rail system, the model can be classified into two submodels, the metro vehicle-track coupling dynamic model and the refined model of fastener system, as shown in Figures 2(a) and 2(b),

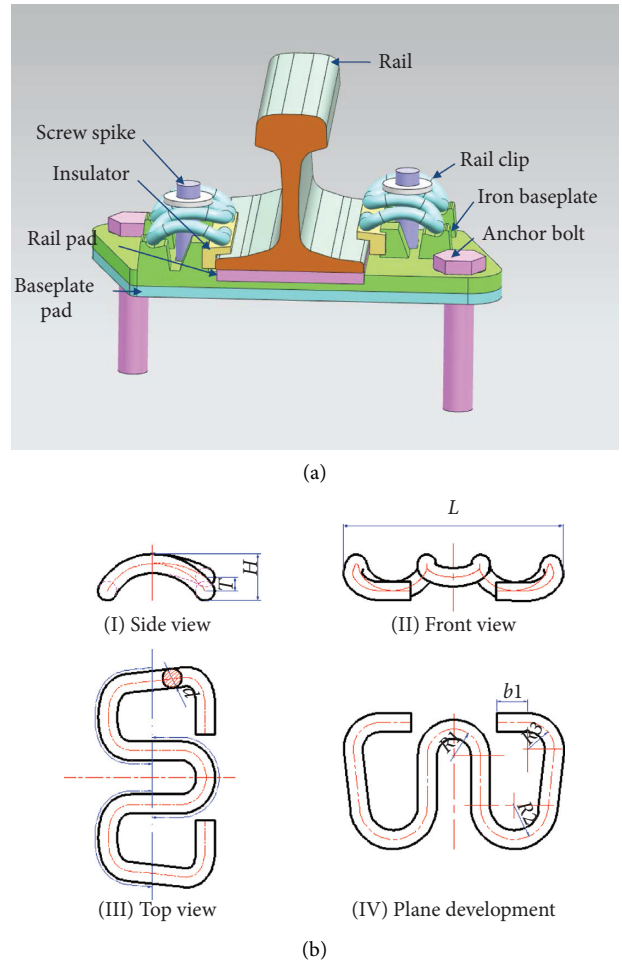

Figure 1: Schematic diagram of the novel fastener system: (a) assembly drawing for fasteners; (b) two-dimensional plan for the elastic rail clip.

respectively. The displacement of the rail is used to connect the two systems. The vehicle-track coupling dynamic analysis is carried out first, to calculate this displacement. The displacement of rail is then imposed on the refined model of the fastener system. In [12, 13], the calculation of specific modeling and wheel-rail contact related to the metro vehicle-track coupling dynamic model is well detailed. Table 1 lists the inertia characteristics and suspension parameters of Metro Type A in China, which are among the important parameters that affect the rail vibration of the metro model.

The fastener system is an assembled body constituted by multiple components. The rail pad is laid between the rail and the iron baseplate, and the baseplate pad is laid between the iron baseplate and the sleeper, both of which have certain elastic and insulating properties. The iron baseplate is a metal component that supports the rail and is fixed on the supporting structure. The insulator is a unit used to transfer transverse forces and adjust the gauge. The anchor bolt is used to fix the iron baseplate. The screw spike is used to fix the clip. The elastic rail clips have contacts with other components and therefore, they affect each other. To

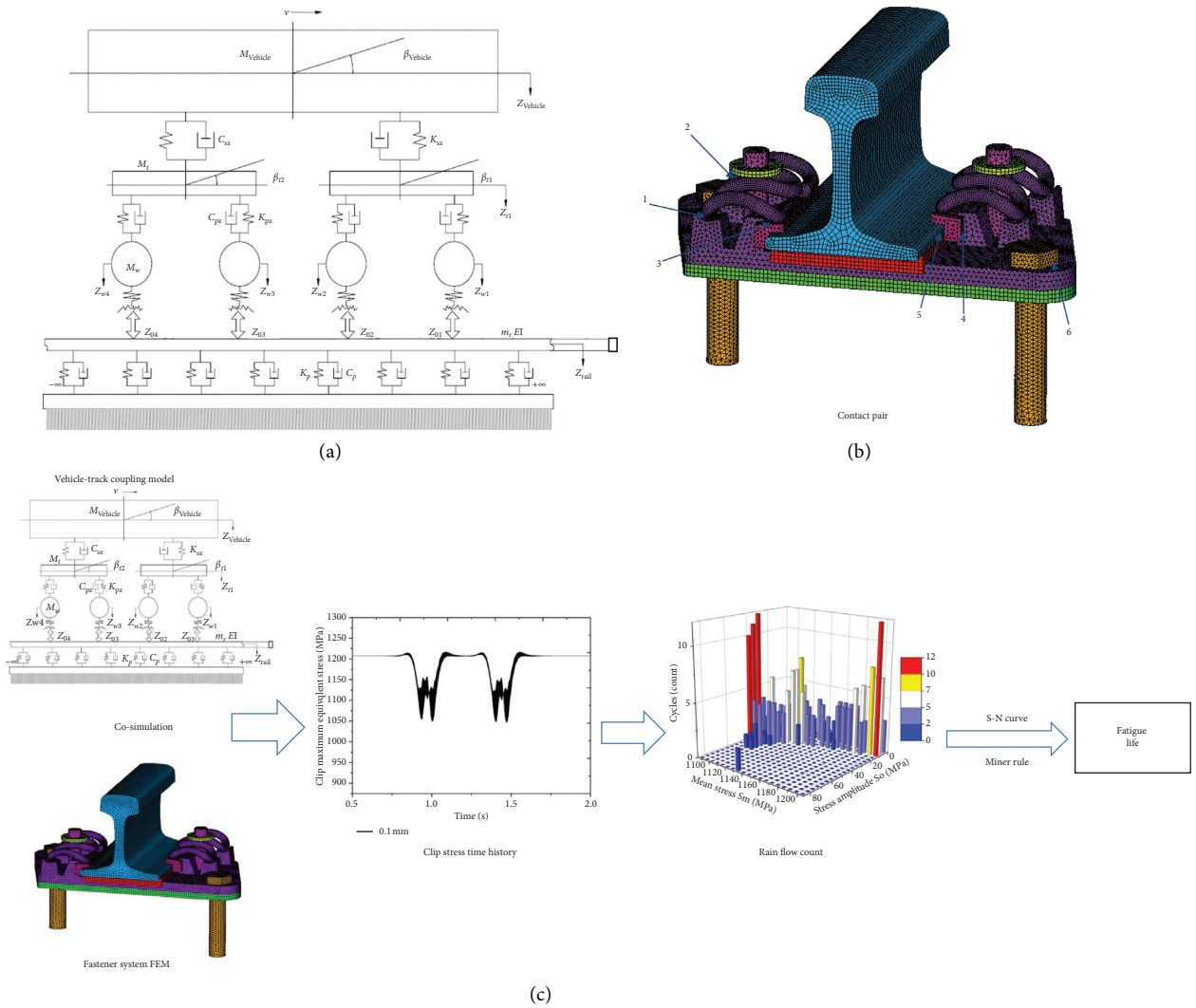

Figure 2: Calculation model and procedures of fatigue life of fastener Elastic rail clips: (a) metro vehicle-track coupling dynamic model; (b) refined model of fastener system; (c) flow chart of calculation of fatigue life.

Table 1: Metro vehicle parameters.

Vehicle parameters	Unit	Symbol	Parameter value
Vehicle body mass	kg	M_{vehicle}	50878
Frame mass	kg	M_t	2721
Wheelset mass	kg	M_w	1900
Vehicle pitch inertia	kg·m^2	J_{vehicle}	4.446×10^6
Frame pitch inertia	kg·m^2	J_t	3605
Primary suspension vertical stiffness	N/m	K_{pz}	4.14×10^6
Secondary suspension vertical stiffness	N/m	K_{sz}	4.5×10^6
Primary suspension vertical damping	N·s/m	C_{pz}	4.9×10^4
Secondary suspension vertical damping	N·s/m	C_{sz}	1.96×10^5
Half-distance between two bogies	m	l_c	7.85
Half-distance between wheel-sets of a bogie	m	l_t	1.25
Wheel radius	m	R	0.42

compare the stress state under the real simulation working conditions of elastic rail clips, finite element software is used to develop the refined model of the fastener system and solid elements are adopted for all components. Considering the contacts between the elastic rail clips and other components, contact pairs are established between elastic rail clips and the iron baseplates, elastic rail clips and insulators, iron baseplates and insulators, insulators and rails, screw spikes and elastic rail clips, and anchor bolts and iron baseplates, as shown in Figure 2(b). The contact element is CONTA174

and the target element is TARGE170. The surface-to-surface contact in soft-soft contact is used for all contact pairs, and the Augmented Lagrange method is selected as the contact algorithm. The parameters of the contact pairs are shown in Table 2. The other components are connected by bonding command. The lower surface of the baseplate pad is under complete constraint, so the influence of the sleeper structure is neglected. By imposing displacement to the screw spikes, the elastic rail clips are considered to be correctly assembled when the displacement of the elastic rail clips reaches 10 mm.

The yield strength and ultimate strength of the elastic rail clip are dependent on its material. Currently, 38Si7 spring steel and 60Si2Mn spring steel are generally used as the materials for elastic rail clips. In accordance with GB/T 1222-2016 Spring Steel Specifications [14], the yield strength and tensile strength of 60Si2Mn spring steel are 1400 MPa and 1600 MPa, respectively, whereas they are 1200 MPa and 1300 MPa, respectively, for the 38Si7 spring steel. The ideal linearly enhanced elastic-plastic model is selected as the material for elastic rail clips, and the reinforcement modulus is 0.1*E*. Under the metro load effect, the elastic rail clips are exposed to stresses in all directions. The Fourth Strength Theory combines the effects of the three principal stresses for consideration and describes the actual stress state much clearer. Hence, the Fourth Strength Theory, the Mises Criterion, is employed to control and evaluate the stresses on the elastic rail clips. The material properties of each component of the refined model of the fastener system are listed in Table 3.

The flow chart of the time domain method for calculating the fatigue life of the fastener elastic rail clips is shown in Figure 2(c). Firstly, the time history curve of maximum von Mises stress of the elastic rail clips under the corrugation effect of the steel rail is obtained through the combined simulation of the metro vehicle-track coupling dynamic model and the refined model of fastener system. Secondly, the number, amplitude, and mean of the fatigue cycles of the fastener elastic rail clips, when a coach passes through, are calculated by the rain flow counting method. Finally, the fatigue life of the elastic rail clips is determined according to the *S-N* curve and the fatigue damage accumulation theory of materials for elastic rail clips.

The elastic rail clip for fatigue load test of constant amplitude bending, made in a smooth round (stress ratio, $R = -1$), is made of 60Si2Mn spring steels. The relationship between the amplitude of the fatigue load and fatigue life is obtained. The *S-N* curve with a survival rate of 95% [15] is as follows:

$$\lg N = 39.59 - 11.84 \lg S_a. \quad (1)$$

On the other hand, the *S-N* curve with a survival rate of 95% [6] for the elastic rail clips made of 38Si7 is as follows:

$$\lg N = 30.36 - 11.7 \lg S_a, \quad (2)$$

where $S_a = (S_{max} - S_{min})/2$ denotes the amplitude of cyclic stress, S_{max} and S_{min} are maximum and minimum stresses (MPa), respectively, and N denotes fatigue life, cycle.

The *S-N* curve of elastic rail clip material is the relationship between the amplitude of the cyclic stress and the fatigue life when the stress ratio $R = -1$, i.e., the mean stress $S_m = (S_{max} + S_{min})/2 = 0$. The elastic rail clip has an initial clamp force at work and its mean stress is not zero. In other words, the elastic rail clip is subjected to asymmetric fatigue load and the effect of mean stress on its fatigue life should be considered. Due to the simplicity and the conservative nature of the model, the Goodman model [16] is generally selected to correct the effect of mean stress on the fatigue life in engineering:

$$\frac{S_a}{S_a(R = -1)} + \frac{S_m}{S_u} = 1, \quad (3)$$

Table 2: Contact pair parameters.

No.	Contact pair	Contact behavior	Contact surface	Target surface	Friction coefficient
1	Clip back end-iron baseplate	Friction	Contact surface of elastic rail clip	Iron baseplate	0.3
2	Clip middle leg-screw spike	Friction	Contact surface of elastic rail clip	Screw spike bottom surface	0.3
3	Clip toe end-insulator	Friction	Clip toe end bottom surface	Insulator top surface	0.7
4	Insulator-baseplate	Binding	Insulator side	Baseplate side	—
5	Insulator-rail	Binding	Insulator bottom surface	Rail bottom surface	—
6	Anchor bolt-iron baseplate	Binding	Anchor bolt bottom surface	Iron baseplate top surface	—

Table 3: Material parameters of each component.

Component	Material	Elasticity modulus (MPa)	Poisson's ratio	Density ($kg \cdot m^{-3}$)
Iron baseplate	QT450-10	1.73*e*5	0.3	7800
Rail clip	60Si2Mn/38Si7	2.06*e*5	0.3	7800
Baseplate pad	TPEE	6	0.45	1190
Rail pad	TPEE	6	0.45	1190
Rail	High manganese steel	2.06*e*5	0.3	7800
Insulator	Glass fiber reinforced Polyamide 66	6200	0.35	1400
Anchor bolt	High manganese steel	2.06*e*5	0.3	7800
Screw spike	High manganese steel	2.06*e*5	0.3	7800

where S_m denotes the mean stress, S_u the tensile strength, S_a the actual stress amplitude when the mean stress is S_m, and $S_a(R=-1)$ the von Mises stress amplitude under the same life when $R=-1$.

The trainload on the elastic rail clips changes with time. By rain flow counting method, the measured load process is simplified into several load cycles to obtain the cycle index of the elastic rail clips under different fatigue stress when a train passes. According to the Miner linear cumulative damage theory [17], the damages caused by different stresses are assumed to be independent of each other. Damages are caused to the materials in each cycle and failure occurs when these damages exceed a critical level. Under the effect of stress level S_{ai}, the damage on the elastic rail clips in n_i cycles is given by $D_i = n_i/N_i$. Hence, the total damage on the elastic rail clip for n_i cycles under r stress levels is given by

$$D = \sum_{i=1}^{r} \frac{n_i}{N_i}, \quad (i = 1, 2, \ldots, r). \tag{4}$$

The fatigue life is given by

$$\text{life} = \frac{1}{D}. \tag{5}$$

When $D = 1$, the fatigue failure of elastic rail clips occurs.

3. Analysis of the Simulation Results

The fatigue failure of rail fastener clip is related to the initial stress of the rail clip after installation and the stress amplitude caused by rail corrugation. Hence, static analysis, modal analysis, and dynamic response analysis shall be executed for the elastic rail clips with different materials before fatigue life prediction.

3.1. Static Analysis of Elastic Rail Clips. Based on the refined model of the fastener system, by applying displacement to the screw spikes, the contact force of the front contact area between the clip and the insulator, namely, the clamping force, is obtained, and the clamping force-displacement curve of the elastic rail clip is obtained. When the middle bend of the elastic rail clip completes the 10 mm deformation, it comes in contact with the insulator, which is called three-point contact; hence, the elastic rail clip is installed properly. The von Mises stress distribution and equivalent plastic strain of the elastic rail clips made of 38Si7 and 60Si2Mn in normal installation state are shown in Figure 3.

Figure 3 shows that the maximum von Mises stress occurs at the back bend of the elastic rail clip, in both cases. The stress level of the front two limbs of the elastic rail clip is comparatively low, and a large stress distribution gradient is observed from the forelimb to the back bend. In both cases, the clamping force of the elastic rail clip in a normal state approximately equals 10.07 kN. This may be because most parts of the elastic rail clip are elastically stressed, while differences are only present in the back bend. For the 38Si7 elastic rail clip, the maximum von Mises stress in the back bend of the spring rail clip is 1209 MPa. This stress exceeds the yield limit of the rail clip material (1200 MPa), and plastic deformation is observed in the back bend. Figure 3(b) shows that plastic yield occurs in a small part of the elastic rail clip, and the maximum yield point occurs inside of the back bend of the elastic rail clip. The maximum plastic strain is about 0.00015. For the 60Si2Mn elastic rail clip, the maximum von Mises stress in the back bend of the rail clip is 1240 MPa. This stress is less than the yield limit of the spring material (1400 MPa), and no plastic deformation is observed in the back bend. Therefore, the strength surplus of the 60Si2Mn elastic rail clip is larger than that of the 38Si7 elastic rail clip.

3.2. Modal Analysis of Elastic Rail Clips. Resonance of the elastic rail clip is observed when the high-frequency excitation generated by rail corrugation is consistent with the natural frequency of the elastic rail clip. According to the modal analysis of elastic rail clips made of two materials and installed in a normal state, the natural frequency of both rail clips within 2000 Hz is basic unanimously. This is because the forces on the two elastic rail clips are almost identical, with the only differences being in the stress concentration areas of the back bends. The natural frequencies of the first two orders are 532 and 651 Hz, respectively, and the modes of vibration are shown in Figure 4.

3.3. Dynamic Response Analysis of Elastic Rail Clips. To study the impact of short-pitch rail corrugation on the new elastic rail clip dynamic response, a rail displacement time curve of a train under rail corrugation was obtained using the metro vehicle-track coupling model. Using the curve as the input for the refined fastener system model, the vertical vibration acceleration response of the elastic rail clip under rail corrugation was obtained. To reveal dynamic characteristics of the clip, the acceleration refers to the acceleration of the highest point of the clip arm. The natural frequencies, vibration performances, and dynamic responses of the elastic rail clips made of the two materials are approximately consistent. Short wavelengths of 30, 40, 50, and 120 mm were selected and used to calculate the vertical vibration acceleration response of the elastic rail clip at a rail corrugation amplitude of 0.1 mm and a train speed of 120 km/h, as shown in Figure 5. At wavelengths of 30, 40, 50, and 120 mm, the maximum vertical vibration acceleration responses of the elastic rail clip are 825, 956, 2260, and 20 m/s^2, respectively. At a train speed of 120 km/h, the wave corrugation excitation frequencies at wavelengths of 30, 40, 50, and 120 mm are 1111, 833, 666, and 277 Hz, respectively. At a wavelength of 50 mm, the vibration frequency of rail corrugation is close to the natural frequencies of the first two orders of the elastic rail clip. This similarity causes resonance, which results in a distinctly increased vibration acceleration. The calculated maximum vibration accelerations of the elastic rail clip at rail corrugation amplitudes between 0.05 and 0.5 mm are shown in Figure 5(e). At a constant corrugation amplitude, the vibration acceleration reaches a maximum when the wavelength of the elastic rail clip is 50 mm and decreases in order at wavelengths of 40, 30, and 120 mm.

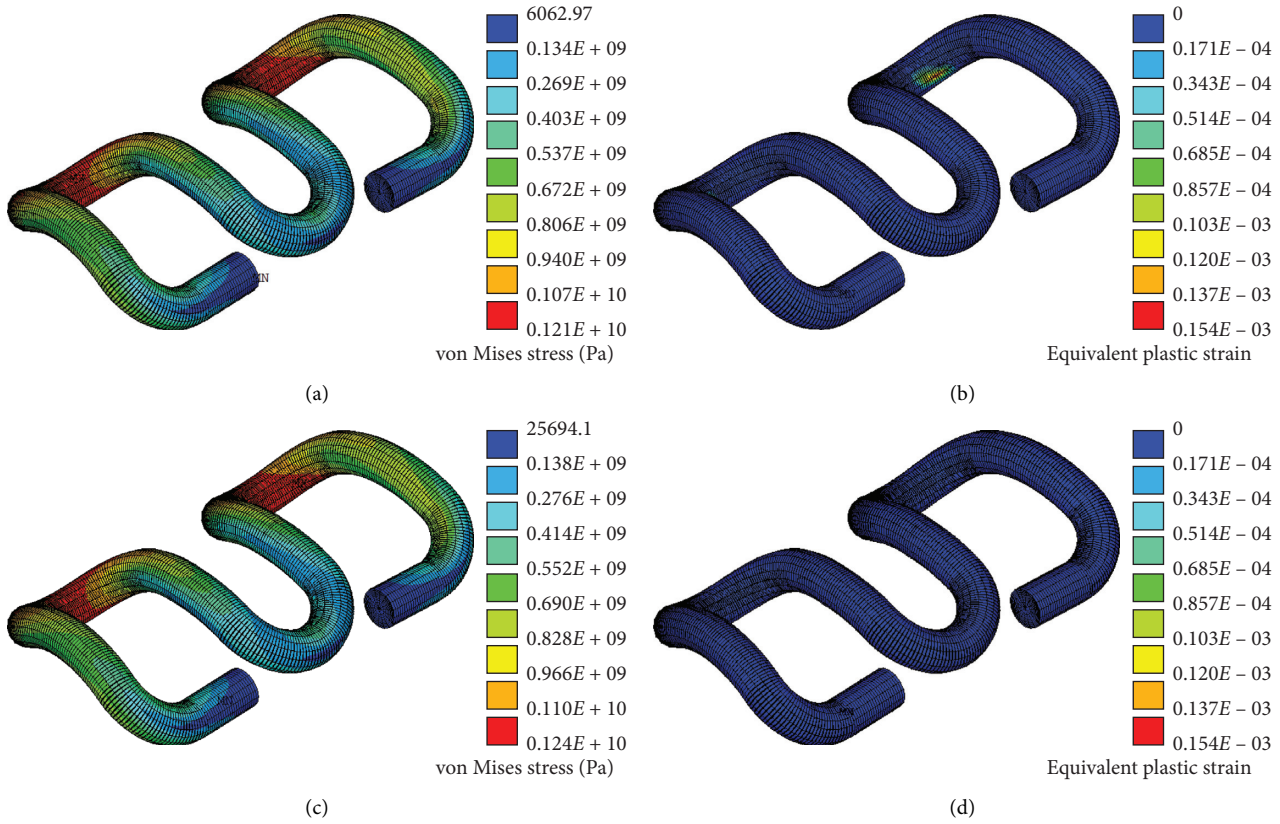

Figure 3: Contour plots under a normal installation state: (a) von Mises stress contour plot of 38Si7 elastic rail clip; (b) equivalent plastic strain contour plot of 38Si7 elastic rail clip; (c) von Mises stress contour plot of 60Si2Mn elastic rail clip; (d) equivalent plastic strain contour plot of 60Si2Mn elastic rail clip.

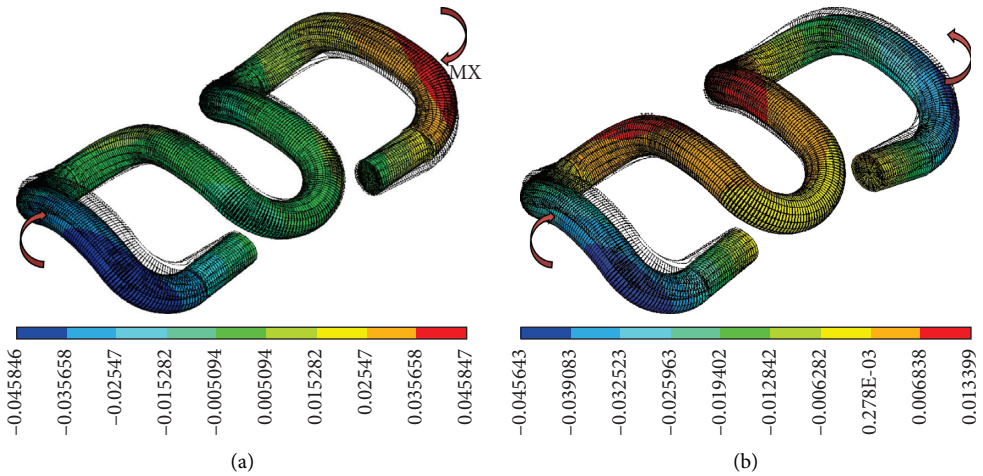

Figure 4: Vibration modes of elastic rail clips under normal installation: (a) first-order vibration mode; (b) second-order vibration mode.

3.4. Analysis of the Influence of Vibration Fatigue Life of Elastic Rail Clips. To analyze the resistances of elastic rail clips made of the two materials to short-pitch rail corrugation, wavelengths of 30, 40, 50, and 120 mm were investigated, and the fatigue lives of elastic clips with rail corrugation amplitudes of 0.05, 0.1, 0.2, and 0.5 mm were calculated. The vehicle speed was 120 km/h. First, the cosimulation was carried out based on the metro vehicle-track coupling and refined fastener system models to determine the stress-time curve of the elastic rail clip at dangerous points. Next, the stress amplitudes and mean stresses of the elastic rail clips were obtained by the rain flow counting method. Finally, the fatigue life of the elastic rail clip was obtained by combining the *S-N* curve of the elastic rail clip material and the theory of fatigue damage accumulation.

The most sensitive wavelength for the new-type elastic rail clip is 50 mm. The maximum von Mises stress-time curve of the 38Si7 elastic rail clip, shown in Figure 6, was

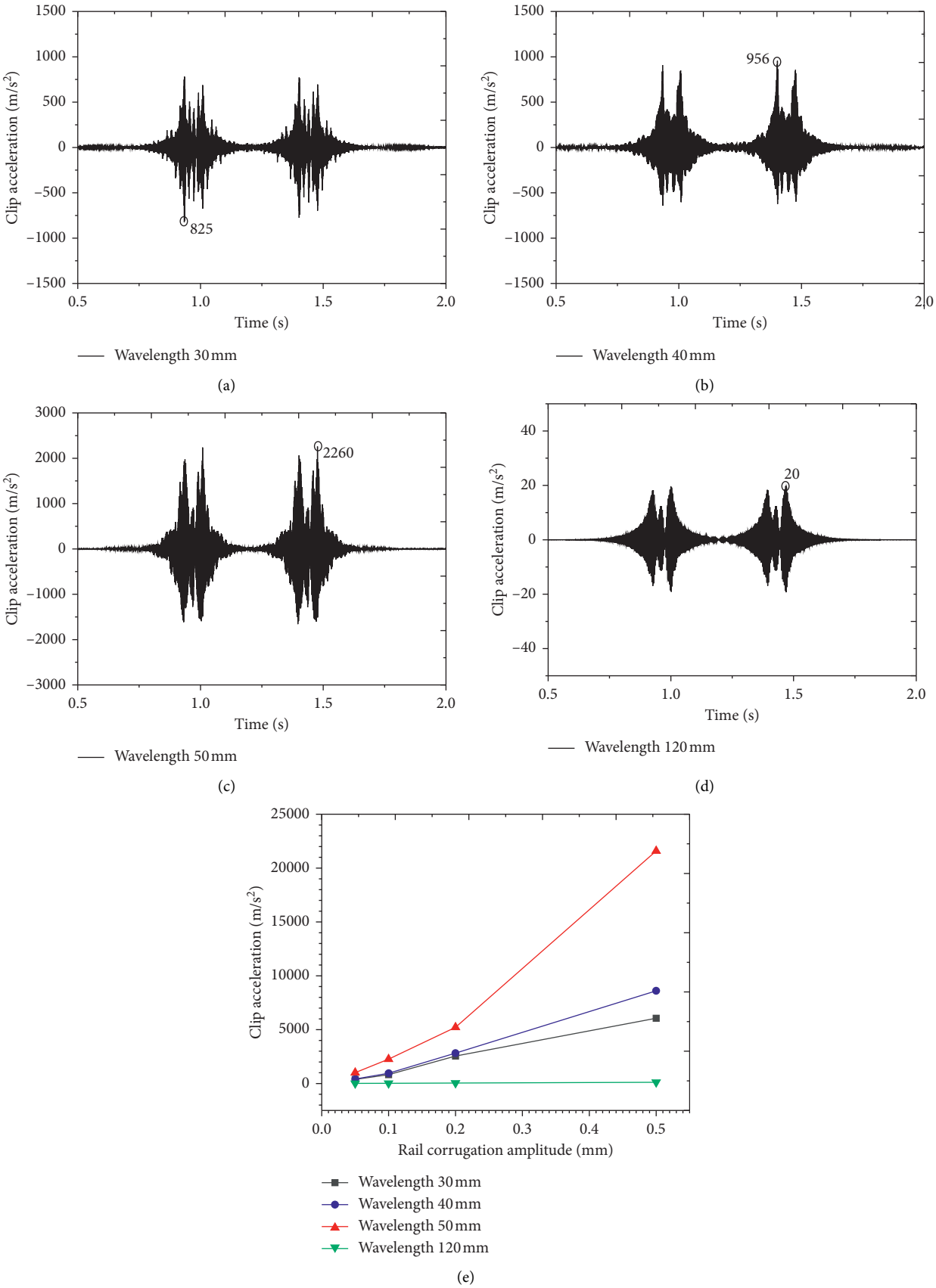

Figure 5: Vibration acceleration of elastic rail clips at different wavelengths: (a) wavelength 30 mm wave depth 0.1 mm; (b) wavelength 40 mm wave depth 0.1 mm; (c) wavelength 50 mm wave depth 0.1 mm; (d) wavelength 120 mm wave depth 0.1 mm; (e) summary.

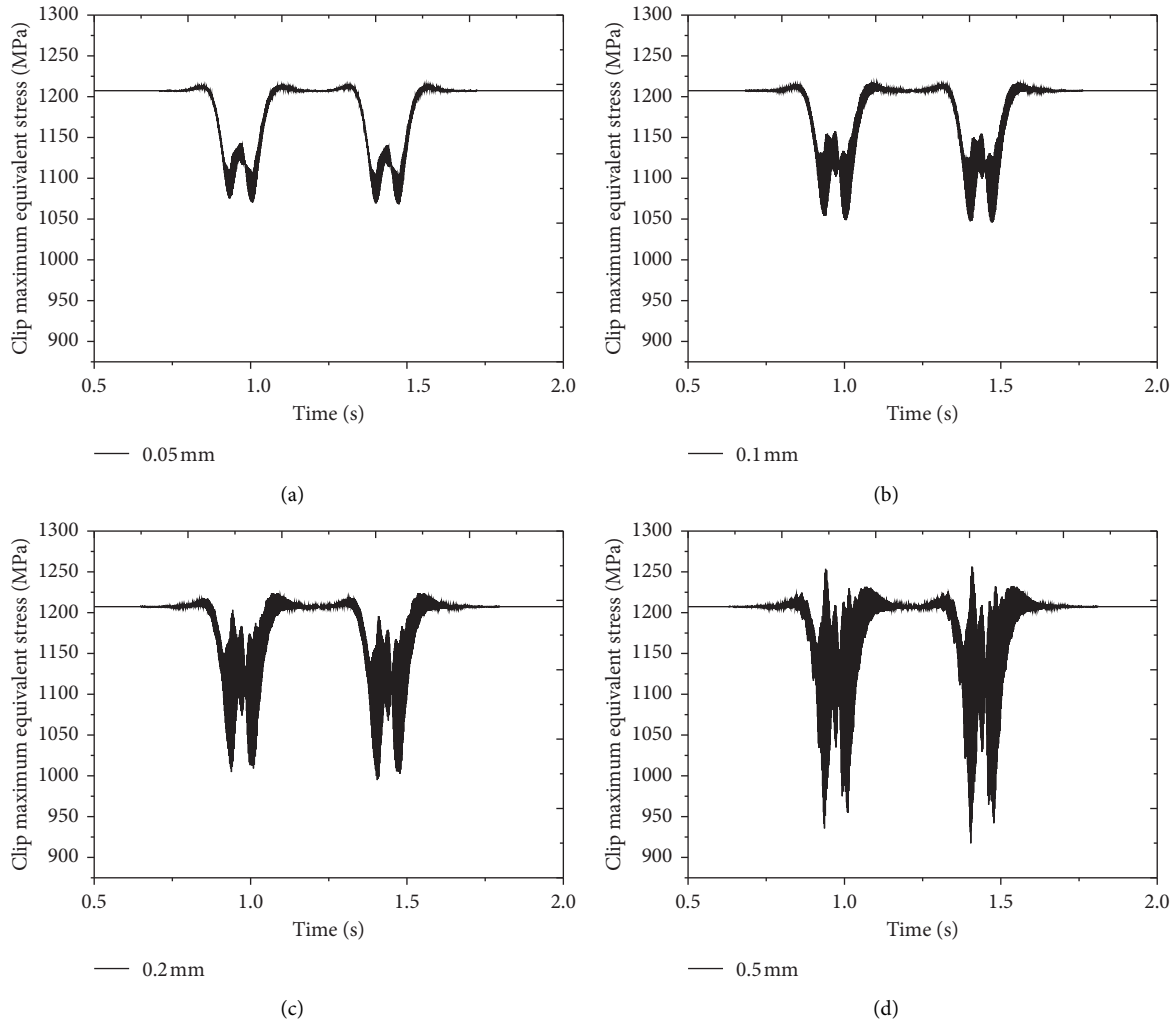

Figure 6: The maximum von Mises stress-time curve of elastic rail clip with a wavelength of 50 mm at different rail corrugation amplitudes: (a) 0.05 mm; (b) 0.1 mm; (c) 0.2 mm; (d) 0.5 mm.

calculated at a wavelength of 50 mm and at amplitudes of 0.05, 0.1, 0.2, and 0.5 mm. In addition to the stress change caused by a moving axle load, stress signals are exposed to superimposition of many high frequencies due to rail corrugation; the amplitude of high-frequency increases with the rail corrugation amplitude, and the stress change of the elastic rail clip is also greater.

The stress amplitude, mean stress value, and cycle times of the maximum von Mises stress of the elastic rail clip at different rail corrugation amplitudes were obtained using the rain flow counting method on the maximum von Mises stress-time curve of the elastic rail clip, and these results are shown in Figure 7. The stress amplitude directly affects the fatigue life of the elastic rail clip. At rail corrugation amplitudes of 0.05, 0.1, 0.2, and 0.5 mm, the maximum stress amplitude is 71, 83, 111, and 165 MPa, respectively. As the rail corrugation amplitude increases, the maximum stress amplitude of the elastic rail clip increases, and a variety of stresses with small amplitudes are added.

Similarly, the calculation for the 60Si2Mn elastic rail clip shows that the dynamic stress change of the elastic rail clip is almost the same as that of the 38Si7 elastic rail clip, with the only differences being in the initial stresses of the elastic rail clips. The fatigue lives of the elastic rail clips, which are based on the number of wheels (two bogies and four wheels in one train), were estimated using the *S-N* curves and the fatigue cumulative damage rule and are shown in Figure 8. As observed, the fatigue lives of both elastic rail clips decrease substantially as the rail corrugation amplitude increases. When the rail corrugation wavelength is 50 mm, the excitation frequency (666 Hz) is the closest to the second-stage natural frequency (651 Hz) of the elastic rail clip. In this case, the fatigue life of the elastic rail clip decreases sharply. The fatigue life of the 60Si2Mn elastic rail clip is longer than that of the 38Si7 elastic rail clip, and this disparity is mainly due to the initial stress and the strength surplus of the 60Si2Mn elastic rail clip. According to the *S-N* curve, the fatigue life of the 60Si2Mn elastic rail clip is longer than that of the 38Si7 elastic rail clip under the same stress amplitude.

For the 38Si7 elastic rail clip, the corresponding corrugation amplitudes at wavelengths of 50 and 40 mm should be controlled below 0.09 and 0.41 mm, respectively, to make the fatigue life of the elastic rail clip exceed 5 million times. For the 60SiMn elastic rail clip, the corresponding

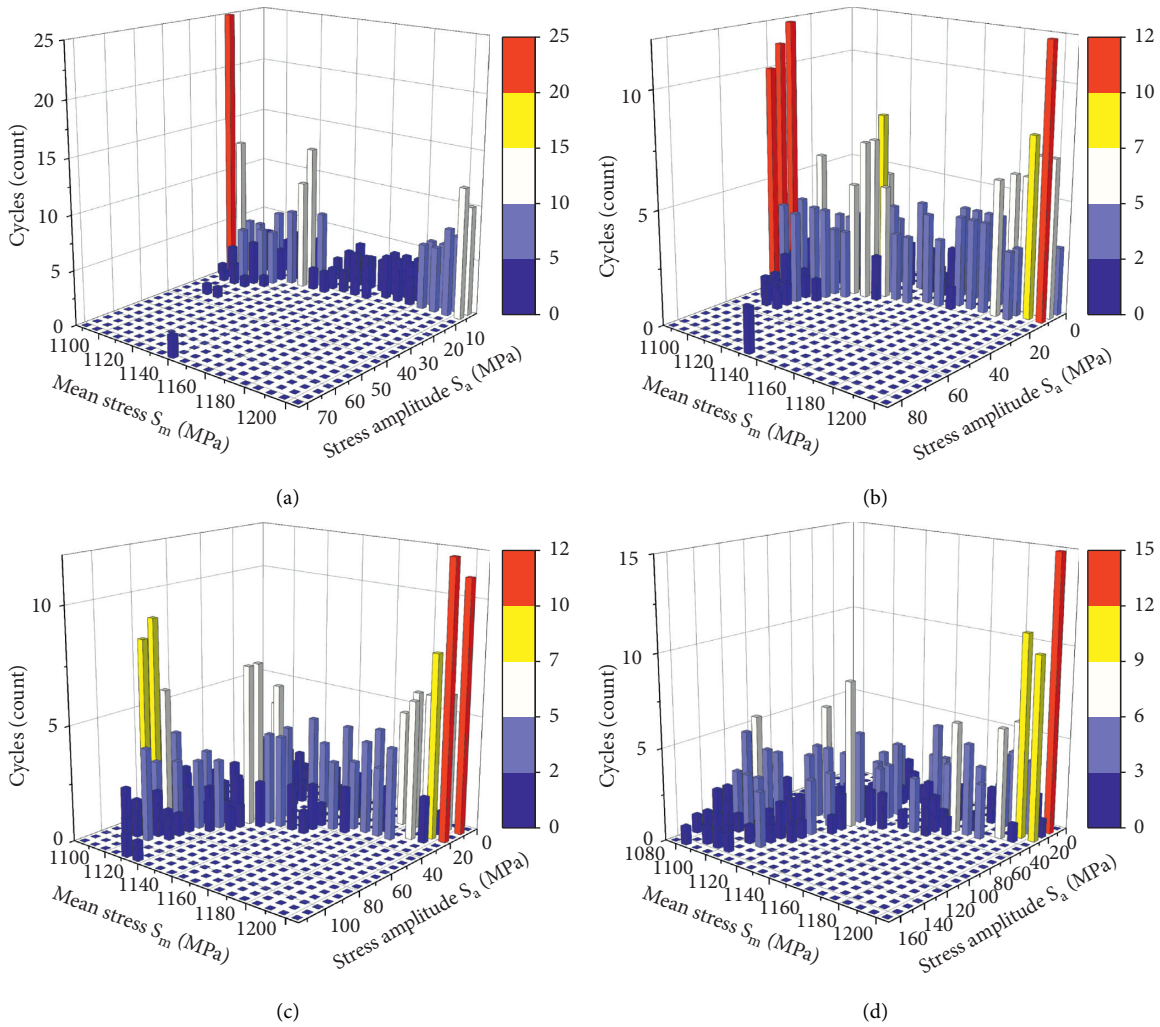

Figure 7: Rain flow counting results for the elastic rail clip with a wavelength of 50 mm at different rail corrugation amplitudes: (a) 0.05 mm; (b) 0.1 mm; (c) 0.2 mm; (d) 0.5 mm.

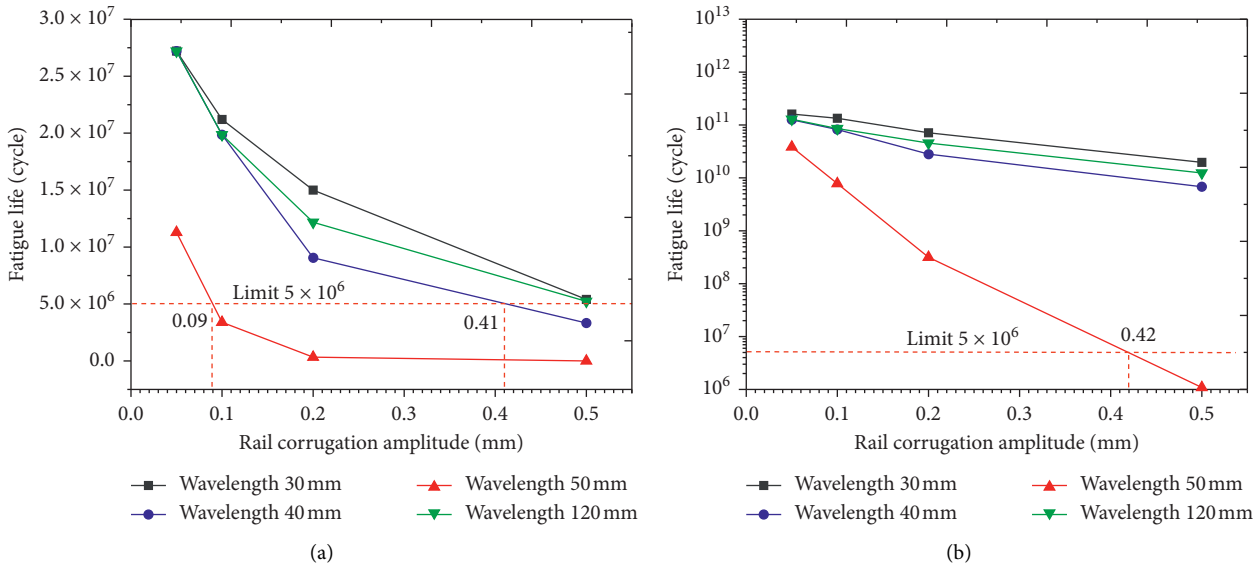

Figure 8: Fatigue lives of elastic rail clips under rail corrugation: (a) 38Si7; (b) 60Si2Mn.

corrugation amplitude at a wavelength of 50 mm should be kept below 0.42 mm to make the fatigue life of the elastic rail clip exceed 5 million times. Considering that the maximum amplitude of rail corrugation at a wavelength of 50 mm is between 0.1 and 0.2 mm according to field test, 60Si2Mn should be selected as it could meet the requirements for fatigue life.

4. Conclusion

This study proposes a novel size-improved elastic rail clip based on the II-type elastic rail clip, a metro vehicle-track coupling dynamic analysis model, and a refined fastening system model. The impact of the elastic rail clip materials (38Si7 and 60Si2Mn) on their static and dynamic responses and the fatigue performance of the elastic rail clips under the impact of rail corrugation were analyzed. The following conclusions can be drawn:

(1) For the 38Si7 elastic rail clip, the maximum von Mises stress at the back bending area is 1209 MPa, which exceeds the yield limit (1200 MPa), and the maximum plastic strain is about 0.00015. For the 60Si2Mn elastic rail clip, the maximum von Mises stress is 1240 MPa. This stress is lower than the yield limit (1400 MPa), and the elastic rail clip is free from plastic strain. The 60Si2Mn elastic rail clip therefore has a larger strength surplus than that of the 38Si7 elastic rail clip.

(2) The clamping forces and natural frequencies (532 and 651 Hz, respectively) of the two elastic rail clips are essentially the same. Meanwhile, the two elastic rail clips have highly similar vibration performances, and they are most sensitive to rail corrugation at a wavelength of 50 mm. At a wavelength of 50 mm and rail corrugation amplitudes of 0.05, 0.1, 0.2, and 0.5 mm, the maximum stress amplitude is 71, 83, 111, and 165 MPa, respectively.

(3) To meet the requirements for fatigue life (5 million times), the corresponding amplitude of corrugation of the 38Si7 elastic rail clip at wavelengths of 50 and 40 mm should be controlled below 0.09 and 0.41 mm, respectively. Elastic rail clips made of 60Si2Mn can meet the requirements on fatigue life. Due to the impact of initial prestress and fatigue performance of the material, the 60Si2Mn elastic rail clip exhibits better fatigue performance than the 38Si7 elastic rail clip.

(4) By expanding the linear size of the elastic rail clip and using high-strength materials, the strength surplus in the back bending area and the resistance of the elastic rail clip to rail corrugation can be enhanced. This study provides references for the performance optimization of the elastic rail clip.

Data Availability

The raw/processed data required to reproduce these findings cannot be shared at this time as the data also form part of an ongoing study. Besides, the novel anticorrugation rail clip in the article is not public now.

Conflicts of Interest

The authors declare that they have no conflicts of interest.

Acknowledgments

Thanks are owed to the National Key Research and Development Program of China (2016YFE0205200) for the research grant awarded to the corresponding author. The work described in this paper was supported by the National Natural Science Foundation of China (U1734207 and 51978585).

References

[1] L. Ling, W. Li, H. Shang, X. Xiao, Z. Wen, and X. Jin, "Experimental and numerical investigation of the effect of rail corrugation on the behaviour of rail fastenings," *Vehicle System Dynamics*, vol. 52, no. 9, pp. 1211–1231, 2014.

[2] J. Xiao and R. Zhao, "Optimization design and study of elastic rail clip fastening," *China Railway Science*, vol. 16, no. 4, pp. 42–47, 1995.

[3] J. Yang and Z. T. C. Pan, "Analysis on influence of elastic rail clip material on fastening performance parameters," *High Speed Railway Technology*, vol. 4, pp. 15–18, 2012.

[4] Z. Li, H. Lin, H. Yan et al., "An investigation on effects on mechanical properties and optimization methods of parameters of ω shape tension clamp," in *Proceedings of the 95th Annual Meeting Transportation Research Board*, Washington, DC, USA, January 2016.

[5] L. Hu, J. Yang, Z. Li et al., "Optimization study of geometric parameters of type W1 elastic rail clip for high speed railway," *Journal of Railway Engineering Society*, vol. 34, no. 12, pp. 24–29, 2017.

[6] S. Mohammadzadeh, S. Ahadi, and H. Keshavarzian, "Assessment of fracture reliability analysis of crack growth in spring clip type Vossloh SKL14," *Proceedings of the Institution of Mechanical Engineers, Part O: Journal of Risk and Reliability*, vol. 228, no. 5, pp. 460–468, 2014.

[7] S. Mohammadzadeh, S. Ahadi, and M. Nouri, "Stress-based fatigue reliability analysis of the rail fastening spring clip under traffic loads," *Latin American Journal of Solids and Structures*, vol. 11, no. 6, pp. 993–1011, 2014.

[8] A. Hasap, P. Paitekul, N. Noraphaiphipaksa, and C. Kanchanomai, "Analysis of the fatigue performance of elastic rail clip," *Engineering Failure Analysis*, vol. 92, pp. 195–204, 2018.

[9] A. Hasap, P. Paitekul, N. Noraphaiphipaksa, and C. Kanchanomai, "Influence of toe load on the fatigue resistance of elastic rail clips," *Proceedings of the Institution of Mechanical Engineers, Part F: Journal of Rail and Rapid Transit*, vol. 232, no. 4, pp. 1078–1087, 2018.

[10] H. Xiao, J.-B. Wang, and Y.-R. Zhang, "The fractures of e-type fastening clips used in the subway: theory and experiment," *Engineering Failure Analysis*, vol. 81, pp. 57–68, 2017.

[11] D. Ferreño, J. A. Casado, I. A. Carrascal et al., "Experimental and finite element fatigue assessment of the spring clip of the SKL-1 railway fastening system," *Engineering Structures*, vol. 188, pp. 553–563, 2019.

[12] J. Lu, M. Gao, Y. Wang, and P. Wang, "Health monitoring of urban rail corrugation by wireless rechargeable sensor nodes," *Structural Health Monitoring*, vol. 18, no. 3, pp. 838–852, 2019.
[13] P. Wang, X. Ma, J. Xu, J. Wang, and R. Chen, "Numerical investigation on effect of the relative motion of stock/switch rails on the load transfer distribution along the switch panel in high-speed railway turnout[J]," *Vehicle System Dynamics*, vol. 57, no. 2, pp. 226–246, 2019.
[14] GB/T 1222-2016, Spring Steel.
[15] Z. Yu, Y. Yuan, Y. Zhang et al., "Study on fatigue property of fastening system of high speed railway," *Journal of Railway*, vol. 36, no. 7, pp. 90–95, 2014.
[16] J. Goodman, *Mechanics Applied to Engineering*, Longmans Green & Co., Harlow, UK, 1918.
[17] M. A. Miner, "Cumulative damage in fatigue," *Journal of Applied Mechanics*, vol. 67, pp. AI59–AI64, 1945.